SRC TR 86-32

Synchrony Supression in Complex Stimlus Responses of a Biophysical Model of the Cochlea

by

S. A. Shamma and K. A. Morrish

Synchrony Suppression in Complex Stimulus Responses of a Biophysical Model of the Cochlea

Authors: Shihab A. Shamma[a,b] and Kathleen A. Morrish[b]

[a] Electrical Engineering Department
& Systems Research Center
University of Maryland
College Park, MD 20742

[b] Mathematical Research Branch
National Institute of Diabetes,
Digestive and Kidney Diseases
National Institutes of Health
Bethesda, MD 20892

Subject Classification: 43.63

Received:

Abstract

A minimal biophysical model of the cochlea is used to investigate the validity of the hypothesis that a single compressive nonlinearity at the hair cell level can explain some of the synchrony suppression phenomena in cochlear responses to complex stimuli. The dependencies of the model responses on the amplitudes and frequencies of two-tone stimuli resemble in many respects the behavior of the experimental data, and can be traced to explicit biophysical parameters in the model. Most discrepancies between theory and experiment stem from simplifications in parameters of the minimal model that play no direct role in the hypothesis. The analysis and simulations predict further results which, pending experimental verification, may provide a more direct test of the influence of the compressive nonlinearity on the relative amplitudes of the synchronous response components, and hence of its role in synchrony suppression. For instance, regardless of the overall absolute levels of a two-tone stimulus applied to this type of model, the ratio of the amplitudes at the input, and the ratio of the corresponding responses at the output, remain approximately constant and equal (the output ratio changes by at most 6 dB in favor of the stronger tone). Other nonlinear responses to multi-tonal stimuli can also be reproduced such, as 'spectral edge enhancement' (Horst et al. (1985), Peripheral Auditory Mechanisms, Springer-Verlag) and some aspects of three-tone suppression (Javel et al. (1983), Mechanisms of Hearing, Monash University Press). In contrast to the complex behavior of synchrony suppression with increasing sound intensity, and the resulting drastic influence of the compressive nonlinearity on the absolute response measures on the auditory-nerve (e.g. average rate and synchrony profiles), the percepts of complex sounds are relatively stable. This suggest that the invarient relative response measures are more likely used in the encoding and CNS extraction of

the spectrum of complex stimuli such as speech.

I. INTRODUCTION

Cochlear function exhibits considerable nonlinear behavior in response to single and complex tonal stimuli. The origin and functional significance of these nonlinearities have been the subject of extensive theoretical and experimental research. One such phenomenon is the mutual suppressive influences exerted by the components of a complex tonal stimulus. This has been variably termed two-tone suppression (or inhibition) when examined using two-tone stimuli (Kim, 1985), rate suppression when the suppressive effects are observed through average rate response measures in the auditory-nerve (Sachs and Kiang, 1968), and synchrony suppression when phase-locked response components are involved (Sachs and Young, 1980; Javel, 1983). It is unclear at present whether these phenomena represent different manifestations of a common nonlinearity, or are due to completely separate mechanisms (Kim, 1985).

Experimental data have been accumulating over the last two decades regarding the detailed behavior of, and parameters important to, these nonlinearities, and several theoretical models have been proposed to account for them. Among the earliest was the phenomenological model of Engebretsen and Eldredge (1968) which dealt with similar suppressive influences observed in cochlear microphonic responses and suggested that multi-tonal interference at a nonlinear (compressive) stage may account for this behavior. Pfeiffer (1970) and Hall (1977) later expanded such a model to account for two-tone inhibition on the auditory nerve. However, objections to this model have been raised based on a variety of later experimental findings (Sellick and Russell, 1979; Kim, 1985) including predictions regarding single tone responses (e.g. the frequency ranking of the saturated portion of the synchrony-level functions). Recently, synchrony suppression has been the focus of many experiments and extensive theoretical conjecture which suggests that its origins lie at the level of the hair cell. Sellick and Russell

(1979), for instance, have demonstrated conclusively its existence in the intracellular responses of the inner hair cells. Furthermore, Javel (1981, 1983, 1984) and Geisler (1985) have proposed phenomenological schemes arguing for a similar origin based primarily on the character of suppression in auditory-nerve fiber responses. However, a detailed theoretical analysis has not yet been carried out to support this hypothesis, to relate it to other cochlear response measures (e.g., frequency tuning curves) and to explicit biophysical parameters. Thus, while the effect of synchrony suppression in shaping the responses of the auditory-nerve to complex sound stimuli is immense (Sachs and Young, 1980), its overall functional significance, its underlying mechanisms, and its relation to other cochlear nonlinearities remain largely uncertain.

In this report, we employ a minimal composite biophysical model of the cochlea to examine synchrony suppression. This model has already been used to describe various linear and nonlinear aspects of cochlear responses to single tones (Shamma et al., 1986). The model consists of a linear basilar membrane, a linear fluid-cilia coupling stage, and a nonlinear inner hair cell model. Our objective here is two-fold: first, to determine the extent to which a single compressive nonlinearity, combined with other linear cochlear stages, can account for various experimental data using two-tone and multi-tonal stimuli, and to use the mathematical model to suggest further experimental tests of this hypothesis; second, to discuss in light of our theoretical model results the possible functional role of synchrony suppression and its potential use in the study of other cochlear nonlinearities.

II. THE MODEL AND METHODS OF ANALYSIS

The model used in this study is based on explicit biophysical descriptions of the various cochlear stages (Shamma et al., 1986). Under specific assumptions, the model's operations can be schematically approximated by the block diagram of Fig. 1 over a wide range of intensities. The first stage is a linear, three dimensional model of basilar membrane mechanics (Chadwick, 1985). The membrane's response at a given location, s, produces inner hair cell cilia displacements via a high-pass fluid-cilia coupling stage. The cilia movements are transduced into intracellular hair cell potentials through nonlinear conductance changes in the apical membrane of an inner hair cell model. The final outputs are studied in terms of the amplitudes of the different frequency components in the intracellular potential waveform. These are discussed with reference to experimentally recorded hair cell potentials and auditory-nerve fiber responses.

In the model, the complex cilia displacement waveform due to a multi-component stimulus may produce a significantly distorted intracellular potential waveform because of the compressive nonlinear transduction of the hair cell. Consequently, the magnitudes of the frequency components of the waveform undergo complicated transformations which will be shown to resemble in some respects the experimentally observed phenomenon of synchrony suppression. In the analyses and discussions of the following two sections, we shall isolate two factors that account for this behavior in the model: (1) the input/output functions of the nonlinear hair cell stage which are mostly determined by the amplitudes (rather than the frequency or phase) of the different frequency components of the cilia displacement waveform; (2) the transfer functions of the basilar membrane and the fluid-cilia displacements which are the primary factors responsible for the frequency dependence of the suppression. We will illustrate these conclusions using two-tone stimuli (Section III), and later extend the analysis to multi-tonal

stimuli (Section IV.). Finally, we discuss the implications of synchrony suppression and its origins for the various response measures and schemes of stimulus spectrum encoding on the auditory-nerve (Section V.).

III. TWO-TONE RESPONSES

In order to simplify the presentation, we shall first discuss the transfer characteristics of the nonlinear inner hair cell model (Part A), and later introduce the additional effects of the linear basilar membrane and coupling stages (Part B).

III.A Transfer Characteristics of the Inner Hair Cell Model

Cilia displacement waveforms representing two-tone stimuli are used to compute the transfer characteristics of the isolated hair cell model. The mathematical formulations underlying the biophysical model and all computations are developed in detail in (Shamma et al., 1986). The basic equation is

$$(C_a + C_b)\, dV/dt + G(u)\,(V-E_t) + G_k\,(V-E_k') = 0 ,$$

where all terms are defined in the Appendix. This equation is used in the computations of all the curves discussed in this section. In order to facilitate a more intuitive presentation of the results, the hair cell model can be approximated over a wide range of intensities by the dimensionless equation (3.1a) (Shamma et al., 1986) where the nonlinear conductance is decoupled from the low-pass filter of the membrane (as shown in Fig.1):

$$\tau \frac{dv}{dt} + v = \tilde{g}(u(t)) , \qquad (3.1a)$$

where

$$\tau = (C_a+C_b)/(G_o+G_k)$$

$$v = \tilde{V}(G_o+G_k)/(\beta G_{max}(E_t-V_o))$$

$$\tilde{g} = \tilde{G}/\beta G_{max}$$

$$V_o = (G_o E_t+G_k E_k')/(G_o+G_k)$$

$$\beta = \exp(-G_1/RT_o)$$

$$\tilde{G} = G(u) - G_o$$

$$= (G_{max}\cdot \beta e^{au} / (1+ \beta e^{au})) - (G_{max}\cdot\beta / (1 + \beta)), \quad \text{(Shamma et. al, 1986)}$$

and all other constants are explicit biophysical parameters defined in the Appendix and (Shamma et al., 1986). Let the cilia displacements, u(t), due to a two-tone stimulus (tone-A + tone-B) be

$$u(t) = A_{in} \sin(\omega_a t) + B_{in} \sin(\omega_b t + \alpha)$$

$$\equiv u_a + u_b ,$$

where

A_{in}, B_{in} = amplitudes of cilia displacements due to the two tones

ω_a, ω_b = frequencies of the two tones taken to be integral multiples of 100 Hz

α = arbitrary phase.

u(t) is thus a linear sum of the displacements produced by each tone separately. In the overall composite model, A_{in} and B_{in} are determined from the levels of the external stimulus using the transfer functions of the basilar membrane and fluid-cilia coupling. The resulting intracellular potential will be a compressed, lowpass-filtered version of the u(t) compound waveform. As an output measure of the response, we Fourier analyze the waveform over the period of the fundamental frequency (100 Hz) and examine the amplitudes of the primary output components (A_{out}, B_{out}) at ω_a and ω_b as functions of A_{in} and B_{in}. These output measures are

not entirely suitable for characterizing completely the effects of the underlying nonlinear transfer functions; however, they have been widely used in experimental studies and hence extensive data are available.

The results of the computations are summarized in Figs. 2(a-b). In Fig. 2a the effects of tone-B (700 Hz) on the synchrony-level (S/L) functions of tone-A (600 Hz) are presented. In the absence of a second tone (B_{in}=0), the S/L function displays the usual linear rise (unity slope on a log-log scale) and saturation with increasing levels of A_{in}. As the level of B_{in} increases, the S/L functions are progressively altered. Two important features are observed: the S/L functions appear to shift horizontally, and their rising slopes remain unaltered (i.e., independent of the interfering tone-B). Both of these features have been noted frequently in the experimental literature (Javel 1981, 1983) and in theoretical models employing compressive nonlinearities (Engebretson and Eldredge, 1968). The first effect of tone-B has been interpreted as increasing the linear range of A_{out} responses (Engebretson and Eldredge, 1968), as suppressing them (Sachs and Young, 1980), or as capturing the unit responses (Geisler, 1985; Javel, 1983). The apparent suppressive effect of tone-B on the tone-A responses has led to the use of the term "synchrony suppression".

The suppressive influences in the responses to two-tone stimuli are not unilateral, but rather reciprocal. That is, while tone-B suppresses A_{out} in Fig. 2a, its own output responses, B_{out}, are simultaneously reduced by A_{in}. Fig. 2b depicts the growth of B_{out} suppression by an increasing A_{in} for the five B_{in} levels considered in Fig. 2a. Thus, when A_{in} is small, B_{out} reduction is negligible. As A_{in} approaches B_{in}, B_{out} begins to decrease (note that here both A_{out} and B_{out} are depressed). For $A_{in} >> B_{in}$, suppression becomes approximately linear.

The suppression of B_{out}, when $A_{in} >> B_{in}$, is entirely analogous to the opposite situation ($B_{in} >> A_{in}$) and hence equally describes the A_{out} reductions (or S/L function shifts) in Fig. 2a[1].

The origin of these hair cell nonlinear transfer characteristics can be understood in the context of the simplified, decoupled model of Fig. 1 and Eq. (3.1a) where the primary role is played by the nonlinear form of the transducer element. Using Eq.(3.1a) we can determine analytically the D.C. component of the intracellular potential response, and the primary A.C. components, A_{out} and B_{out}. For the D.C. component, the τ dv/dt term does not contribute, and hence the D.C. component can be evaluated from the remaining dimensional form of the equation as follows. From the definitions in Eq.(3.1a), we have

$$v = \tilde{V}(G_o+G_k)/\beta G_{max}(E_t-V_o)$$

and
$$v = \tilde{g} = \tilde{G}/\beta G_{max} = (G(u)-G_o)/\beta G_{max} = (e^{au} / (1+\beta e^{au})) - 1/(1+\beta).$$

Combining the above two equations we get:

$$\tilde{V} = \text{intracellular potential deviations from rest}$$

$$= C_o \frac{\beta e^{au}}{1 + \beta e^{au}} + C_1 \equiv C_o\, g(u) + C_1 , \qquad (3.1b)$$

where

$$C_o = \frac{G_{max}(E_t-V_o)}{G_o + G_k}$$

$$C_1 = \frac{-\beta}{1+\beta} C_o \ .$$

---

[1]None of the response features described in Figs.2 are dependent on the frequency or phase of the two tones, provided certain conditions are satisfied. These conditions are discussed with reference to Eq.3.2 in the text.

Therefore, the D.C. response is the average intracellular potential over one period of the response:

$$\tilde{V}_{DC} = C_o\,[g(u)]_{DC} + C_1 \ ,$$

where $$[g(u)]_{DC} = \frac{1}{T}\int_T g(u)\,dt \ .$$

The primary A.C. components can be readily evaluated from Eq.(3.1b) and the additional attenuation, $k(\omega)$, due to the low-pass filter of the hair cell membrane (via the $\tau\, dv/dt$ term in Eq.(3.1a)):

$$A_{out} \equiv \left|\tilde{V}_{AC}\,(\omega_a)\right| = [g(u)]_{AC} \cdot C_o \cdot k(\omega_a) \equiv [g(u)]_{AC} \cdot C'(\omega_a)$$

$$B_{out} \equiv \left|\tilde{V}_{AC}\,(\omega_b)\right| = [g(u)]_{AC} \cdot C_o \cdot k(\omega_b) \equiv [g(u)]_{AC} \cdot C'(\omega_b) \ ,$$

where $$k(\omega) \equiv 1 \,/\, \sqrt{1 + (\omega\tau)^2}$$

$$[g(u)]_{AC} = \left| \frac{1}{T}\int_T g(u)\ e^{-j\omega t}\,dt \right|$$

= magnitude of the Fourier component at ω, where T is the fundamental period of the stimulus and $j = \sqrt{-1}$.

First, consider the case where one of the tones (e.g., u_a) is small. Then

$$g(u) = g(u_a + u_b) \approx g(u_b) + g'(u_b)\cdot u_a,$$

where $$g'(u_b) = \left.\frac{dg(u)}{du}\right|_{u_b} .$$

Therefore, the amplitude of the AC output component due to the smaller tone, A_{out}, is given by

$$A_{out} = \left|\tilde{V}_{AC}(\omega_a)\right|$$

$$= \frac{1}{T}\left| \int_T g(u_b)\ e^{-j\omega_a t}dt \ + \ \int_T g'(u_b)\cdot u_a \cdot e^{-j\omega_a t}dt \right| \cdot C'(\omega_a) \ .$$

If $g(u_b)$ is expanded as a Fourier series, then the first term is small or vanishes if $\omega_b > \omega_a$ (since all products involve orthogonal terms) or if the higher harmonics

of ω_b decrease sufficiently rapidly. When the second term dominates, then

$$A_{out} \approx \frac{1}{T} \left| \int_T g'(u_b) \cdot u_a \cdot e^{-j\omega_a t} dt \right| \cdot C'(\omega_a) \qquad (3.2)$$

$$= (A_{in} / T) \cdot \left| \int_T g'(u_b) \sin(\omega_a t)\, e^{-j\omega_a t}\, dt \right| \cdot C'(\omega_a) \; .$$

This equation describes the relationship between the response of the two tones observed in Fig. 2a. The response to the weaker tone A_{out} is linearly dependent on its input intensity A_{in} regardless of the B_{in} level. The slope of the linear rise (and hence the amount of shift on the log-log scale) are dependent on B_{in} and can be evaluated from Eqs.(3.2) as follows:

$$A_{out} = C'(\omega_a) \frac{A_{in}}{T} \left| \int_T g'(u_b) \frac{1}{2} \sin 2\omega_a t \, dt - j \left\{ \int_T (1/2)\, g'(u_b)\, dt - \int_T g'(u_b) \frac{\cos 2\omega_a t}{2} dt \right\} \right|$$

The 1st and 3rd terms again are small or vanish under the same conditions that led to Eq.(3.2) above. Therefore,

$$A_{out} \approx \frac{A_{in}}{2} \cdot [g'(u_b)]_{DC} \cdot C'(\omega_a) \; . \qquad (3.3)$$

$[g'(u_b)]_{DC}$ is a function of B_{in}. On a log-log plot, it describes the intercept of the A_{out} line, or alternately, the A_{out} variation with B_{in}. Thus, the magnitude of the response A_{out} varies with B_{in} in a complex nonlinear manner described by Eq.(3.3). Since the reciprocal relation holds equally when $A_{in} >> B_{in}$, an expression analogous to Eq.(3.3) then describes the suppression of B_{out} by A_{in} in Fig. 2b.

An intuitive understanding of Eq.(3.3) obtains from its graphical representation in Figs.3, where u_b and the resulting functions, $g(u_b)$ and $g'(u_b)$ are depicted as functions of time. From Eq.(3.3), A_{out} is proportional to the area under $g'(t)$ (shaded in Fig.3b). As B_{in} increases, $g'(t)$ areas (and hence A_{out}) become smaller. The rate of decrease is partially dependent on the form of the

nonlinearity g(u), and can be approximately determined as follows. With reference to Fig.3b, the integral in Eq.(3.3) can be written as the sum of $(2 \cdot T/T_b)$ terms (each representing one of the shaded regions):

$$A_{out} = (A_{in}/2T) \cdot C'(\omega_a) \cdot \left| \sum_{n=1}^{2T/T_b} \int_{T_b/2} g'(u_b)\, dt \right|$$

$$= (A_{in}/2T) \cdot C'(\omega_a) \cdot \frac{2T}{T_b} \cdot \left| \int g'(u_b) \frac{dt}{du_b} \cdot du_b \right| ,$$

where $dt/du_b = 1/(\omega_b \cdot \sqrt{(B_{in}^2 - u_b^2)})$ and $T_b = 2\pi/\omega_b$. Let u_o be the displacement (u) at the point of maximum g'(u) (Fig.3). Then for $B_{in} \gg u_o$ (Fig.3), $g'(u_b)$ approaches a delta function (with respect to u) centered at u_o and the integral can be approximated by the value of $(dt/du_b)|_{u_b=u_o}$:

$$A_{out} \approx (A_{in}) \cdot C'(\omega_a) \cdot (1/T_b) \cdot (1/(\omega_b \cdot \sqrt{(B_{in}^2 - u_b^2)}))$$

$$= A_{in}/2\pi \cdot C'(\omega_a)/B_{in} \cdot 1/\cos(\theta) , \quad \text{where } \sin(\theta) \equiv u_o/B_{in}. \qquad (3.4)$$

It is evident from Eq.(3.4) that the slope of A_{out} suppression may vary depending on the parameters of the nonlinearity (through $u_o(\beta,a)$) and the level of the suppressing tone, B_{in}. For very large B_{in} ($\theta \rightarrow 0$), A_{out} is inversely proportional to B_{in} (with slope -1 on the log-log plot of the analogous situation $A_{in} >> B_{in}$ of Fig.2b). For moderate B_{in} levels, however, θ is approximately equal to u_o/B_{in} ($= (1/a) \cdot \ln(1/\beta) / B_{in}$), and hence the growth rate of A_{out} suppression may exceed unity (on the log-log plot). These results then agree with the experimental findings that the slopes of suppression growth functions typically vary around unity (Javel, 1983), and may relate these variations to the underlying biophysical parameters of the nonlinearity.

In Fig.4, the model responses are viewed from another perspective. Here the change in the relative levels of the two-tone output (A_{out}/B_{out}) is examined as a function of the absolute level of the stimulus, with input level ratio (A_{in}/B_{in}) as a parameter. For low absolute levels, the response is linear and hence the relative levels at the input (A_{in}/B_{in}) and at the output (A_{out}/B_{out}) are expected to be equal. However, for large absolute stimulus levels, the response saturates and become nonlinear. Fig.4 shows that, as the response to the larger tone saturates, A_{out}/B_{out} becomes slightly enhanced ($\leq$6 dB) in favor of the stronger tone; i.e., regardless of the absolute level of the two-tone stimulus, the ratio of the output synchronous components (A_{out}/B_{out}) differs from the input ratio (A_{in}/B_{in}) by no more than 6 dB, in favor of the stronger tone. This asymptotic behavior of A_{out}/B_{out} can be predicted for the case ($A_{in}/B_{in} \ll 1$) from the above analysis (Eq.3.4) and the following expression for the saturated level of the tone-B response, B_{out} :

$$B_{out} = (C'(\omega_b)/T_b) \cdot \left| \int_{T_b} g(u_b)\, e^{-j\omega_b t} dt \right| ,$$

which, for large Bin, can be approximated by (Fig.3a):

$$\begin{aligned} B_{out} &\approx (C'(\omega_b)/T_b) \cdot \left| \int_{t_1}^{t_2} e^{-j\omega_b t} dt \right| \\ &= C'(\omega_b) \cdot \cos(\theta)/\pi , \quad \text{where } \sin(\theta) = u_o/B_{in} . \end{aligned} \tag{3.5}$$

Combining Eqs.(3.4,3.5), we get:

$$A_{out}/B_{out} = \{ (1/2) \cdot C'(\omega_a)/C'(\omega_b) \cdot 1/(\cos\theta)^2 \} \cdot (A_{in}/B_{in}) \tag{3.6}$$

$$\dashrightarrow (1/2) \cdot C'(\omega_a)/C'(\omega_b) \cdot A_{in}/B_{in} \quad \text{for large } B_{in} \ (\theta \dashrightarrow 0).$$

The factor $C'(\omega_a)/C'(\omega_b)$ reflects the relative attenuation of the responses by the low-pass filter of the hair cell membrane; it is approximately equal to 1 for closely spaced frequencies ω_a and ω_b. The simulation illustrated in Fig.4 shows that Eq.(3.6) applies over a wide range of input ratios and absolute levels. It is

also evident that, when $A_{in}/B_{in} = 1$, no significant change in the output ratio should be expected [2]. There are no experimental data available at present to verify the behavior depicted in Fig.4 and hence to test the validity of the assumptions implied by the form of the model.

In summary, the nonlinear compressive action of the hair cell transducer results in reciprocal suppressive interactions between the responses of two tone stimuli. These interactions are reminiscent of hair cell and auditory nerve synchrony suppression phenomena. Moreover, these interactions are primarily determined by the relative input levels to the nonlinear hair cell stage (i.e. cilia displacements). Since the nonlinear conductance acts instantaneously, the suppression effects are largely frequency and phase independent provided the tones involved are not low order harmonics of a common fundamental. However, as we discuss in the next section, frequency dependencies do arise when we include the effects of the basilar membrane and fluid cilia coupling of the overall cochlear model.

III.B Two-Tone Interactions in the Complete Cochlear Model

The frequency dependence of synchrony suppression in the response of the cochlear model stems from two sources: (1) The basilar membrane tuning and fluid cilia coupling, which determine the relative levels of hair cell cilia displacements at the input of the nonlinear stage; (2) The hair cell low pass filter, which attenuates the outputs A_{out} and B_{out} by the factor $k(\omega)$ discussed earlier. The effects introduced by these two factors are explored in Figs. 5a-d,

---

2
Note that, since the cilia displacement levels A_{in}, B_{in} are frequency dependent in the overall composite model (Sec.IV), the case $A_{in}/B_{in} = 1$ does not in general correspond to equal external stimulus levels.

where the iso-intensity AC response curves to tone-A are computed, first alone (Fig. 5a) and second in the presence of a second constant frequency tone-B at three different levels (Figs. 5b-d).

In Fig.5a, the tuned response curves show the experimentally observed nonlinear effects of increasing intensity, namely the broadening of the bandwidth and the downward shift of the BF (Shamma et al., 1986). These changes result from the combined influences of the nonlinearity and the lowpass filter of the hair cell. The same overall features persist in the presence of a second tone (1.7KHz) at different levels (Figs. 5b-d). The only significant change is the lowering of the A_{out} responses with increasing tone-B levels. A_{out} suppression is also accompanied by a decrease in the saturation and downward BF shifts of the tuning curve, due to the effective increase of the linear range of response (as discussed earlier with regard to Fig. 2a). Since the frequency of tone-B determines its effective level at the hair cell input B_{in} (this according to the linear transfer functions of the basilar membrane and fluid cilia coupling), then it is expected that the most effective suppression of A_{out} will occur for tone-B frequencies near the BF of the basilar membrane.

The reciprocal suppression of B_{out} is shown in Figs.6a-c. In each plot B_{out} is computed as a function of tone-A frequency at different levels. As before, the frequency dependence of B_{out} suppression arises from the changing effective level of A_{in} (at the hair cell input). Thus, maximum suppression always occurs when cilia displacements A_{in} are largest, i.e., at the BF of the basilar membrane (or slightly above it due to the high pass filter of the coupling stage). Note also that, since the basilar membrane and fluid-cilia coupling stages are linear, this frequency of maximum suppression remains stable with increasing levels of tone-A.

This is in contrast to the frequency of peak A_{out} response (Fig.5a) which deviates from the basilar membrane BF sigificantly at high levels because of the downward shifts.

Finally, observe that, when tone-B is relatively small, B_{out} suppression is almost independent of the tone's absolute level. Thus, Figs. 6a and 6b appear similar except for an overall vertical shift. This follows directly from Fig.2b where the slopes of B_{out} suppression curves are equal to 1 regardless of the B_{in} level. In summary, the patterns of two-tone responses in the overall cochlear model can be understood in the context of the nonlinear interactions due to the hair cell transducer, and the frequency dependent effects of the linear basilar membrane, fluid-cilia coupling, and hair cell membrane stages. These patterns account for many aspects of synchrony suppression behavior observed in hair cell and auditory nerve recordings; they differ significantly in other respects, however, as we elaborate in the discussion.

IV. Responses to multi-tonal stimuli

The interpretations of the results from the two-tone simulations can be readily extended to explain the output of multi-tonal stimuli. Fig. 7 illustrates a simulated three-tone experiment (Javel, 1984) in which the AC response to a small stationary tone-C (C_{out}) is computed in the presence of two suppressing tones: a steady tone-B and an increasing intensity tone-A. At the two extreme levels of tone-A ($A_{in} >> B_{in}$, $A_{in} << B_{in}$), C_{out} is suppressed by an amount dependent on the larger tone only (regardless of the level of the third tone). This result is expressed by the following relationships for small tone-C and tone-B levels:

$$g(u_a + u_b + u_c) \approx g(u_a) + g'(u_a)\cdot(u_b + u_c)$$

Carrying out the analysis as before (Eq.3.3), C_{out} and B_{out} are then given by

$$C_{out} \approx (C_{in}/2)\cdot[g'(u_a)]_{DC} \cdot C'(\omega_c)$$

$$B_{out} \approx (B_{in}/2)\cdot[g'(ua)]_{DC} \cdot C'(\omega_b)$$

assuming that ω_a, ω_b, ω_c satisfy conditions similar to those that led to Eq.3.2, and in addition, that the sum $\omega_b + \omega_c$ is not an integer multiple of ω_a. Therefore, the suppression of C_{out} is similar to the two-tone case in Section III. This suggests that, in general, a relatively strong component in a complex sound will suppress all other smaller components by about the same amount. When the suppressor tones -A and -B are of comparable amplitudes, however, C_{out} suppression does not add linearly. Instead, C_{out} is given by: $C_{out} = C_{in}/2 \cdot [g'(u_a+u_b)]_{DC} \cdot C'(\omega_c)$, which exhibits a complex dependence on the levels of the two large tones through the $[\ ]_{DC}$ operation. C_{out} may even increase, reflecting a less effective suppression. These trends can be seen in the numerical simulations and in experimental data (Javel, 1984).

The model also accounts for recently observed nonlinear 'spectral edge enhancement' in auditory-nerve-fiber responses to in-phase multi-component stimuli. Here a complex stimulus of the form

$$u(t) = A_{in} \sum_{n=M}^{N} \sin(n\omega_o t)$$

where $\omega_o/2\pi$ = fundamental frequency of the stimulus, is applied to the hair cell model (as in Sec. III.A). The primary synchronous response components ($A_{out}(n\omega_o)$) are computed and plotted in Fig.8 for different overall stimulus levels (A_{in}). At low intensities, the response is linear, and $A_{out}(n\omega_o)$ resembles the transfer function of the hair cell lowpass filter. At high levels, however, u(t) saturates and the spectrum exhibits 'edge enhancement' effects - a direct result of the progressive 'flattening' of the envelope of the u(t) waveform due to the compressive nonlinearity. The 'spectral enhancement' here is qualitatively similar to

the enhancement of the response to the stronger tone observed in the two-tone case (Fig.4). These effects largely persist when the u(t) spectrum is first filtered by the basilar membrane and coupling stages, with the enhancement now occuring instead at the edge frequencies of the filter. Preliminary simulations also show that randomizing the phases of different components (thus modifying the shape of u(t) significantly) removes the enhancement effects, in agreement with experiment (Javel, 1984).

In summary, the response to multi-tonal stimuli exhibit complex and varied behavior when viewed in terms of its synchronous components. Some of these effects can be understood as an extension of the two-tone results, but others are more difficult to analyze in those terms. Undoubtedly, many more such nonlinear changes can be simulated depending on the stimuli and paradigms employed. However, all are manifestations of the same hair cell nonlinearity.

V. Discussion

We have examined the synchronous responses of tonal stimuli in a biophysical model of the cochlea. In particular, we have analyzed the reciprocal suppressive interactions due to a single nonlinearity at the hair cell level. The computations indicate that the resulting patterns of response may account for major features of synchrony suppression that have been observed at the hair cell and auditory nerve levels.

Synchrony suppression behavior in the model originates at the inner hair cell transduction nonlinearity, because of its instantaneous compressive action on the compound waveform of the cilia displacement. Suppression is primarily dependent on the relative levels of the tones at the input of the nonlinearity. Frequency dependence arises only to the extent that (1) the basilar membrane and fluid cilia

coupling transfer functions affect these levels, and (2) the hair cell membrane attenuates the measured intracellular potentials. The qualitative behavior of the computed results is robust and reflects the general form of the transfer characteristics of the model elements. Despite general agreement with experimental data, there are some significant differences which will be mentioned as we discuss two important aspects of synchrony suppression: (1) its relation to cochlear frequency selectivity, and (2) its functional role in complex sound processing. These descrepencies, as we discuss below, are due to simplifications in parameters of the minimal model that do not play a direct role in synchrony suppression, rather than to inherent inadequecies of the hypothetical role of the transduction nonlinearity, and hence cannot be taken as definitive arguments against the hypothesis. Instead, experimental verification of such results as those of Fig.4 provides a more direct test of the influence of the compressive nonlinearity on the relative amplitudes of the synchronous response components, and of its role in synchrony suppression.

Synchrony Suppression and Cochlear Frequency Selectivity

Some aspects of synchrony suppression exhibit frequency dependencies that closely reflect the underlying transfer functions of the various cochlear stages (Javel, 1983). In the model, these dependencies arise from the fact that the levels of the two interacting tones entering the hair cell model are determined by the basilar membrane tuning and fluid-cilia coupling. Much of the experimental data regarding two-tone synchrony suppression and its stimulus levels and frequency dependence can be qualitatively and readily understood within this framework. There are, however, obvious discrepancies. For instance, since the model contains no position-dependent parameters, no BF-dependent changes in the response

patterns can be simulated (Javel 1983). Furthermore, the often observed nonlinear growth of the high frequency slope of the basilar membrane with intensity is absent in this linear model (Evans, 1975).

In order for synchrony suppression to occur in this model, each tone must be able to elicit a separate cilia displacement (and hence an AC intracellular potential). Therefore, synchrony suppression is expected to occur entirely within the AC excitatory field of auditory units, which is in agreement with data from auditory nerve fiber recordings (Javel, 1983). Exceptions to this rule, however, have recently been cited (Deng et al., 1985), suggesting that in some instances a suppressor tone alone may not elicit any auditory-nerve-fiber responses. This result may still be consistent with the model if AC response thresholds of the hair cell are somewhat lower than those of the auditory-nerve (e.g., because of synaptic transmission).

The suppression contours of Figs.6 show a progressive increase in frequency selectivity with increasing levels of suppression. This can be understood with reference to the increasing slopes of the B_{out} suppression functions, with increasing A_{in}, near the 'knees' of the curves in Fig.2b. This behavior may indirectly account for the experimental finding of increased selectivity of the iso-suppression contours with increasing suppression criteria (Sellick and Russell, 1979; Javel 1983). However, the model cannot account for the small, but measurable (Javel, 1983), shifts in the frequency of maximum suppression which suggest that an additional nonlinear source is involved.

Although the emphasis in this report has been on synchrony suppression, we have also computed in all simulations discussed above the DC responses of the model. This measure roughly corresponds to the average rate of auditory-nerve-fiber responses. Under the stimulus conditions imposed in this study (i.e., harmonically related tones with relatively small frequency separations), the DC

behavior exhibited a complex dependence on stimulus levels, frequencies, and phase, and a multitude of other effects including, in some cases, two-tone rate suppression (Javel, 1981).

Finally, it should be emphasized that the single hair cell nonlinearity may exhibit a multitude of other nonlinear responses depending on the stimuli and the experimental paradigms employed. This is particularly true with such response measures as the 'synchrony vector' which, while beneficial in summarizing the transfer functions of linear systems, are generally inappropriate for studying nonlinear phenomena. Therefore, it would not be helpful to try to catalog all such observations, and it would be misleading to treat each one as a manifestation of a 'new' nonlinearity.

The encoding of complex sounds in the presence of the compressive nonlinearity

Until now, we have described the effects of the hair cell saturating nonlinearity mainly in terms of the levels of the primary synchronous components of the response. This has allowed us to compare these results with similar experimental data from hair cell and auditory-nerve-fiber recordings. The complex, but regular, "suppression" behavior that emerges, however, raises two questions: (1) Does the focus on the primary synchronous components (i.e. frequency analysis approach) lead to an unnecessarily complex picture which obscures the global effects of the nonlinearity? (2) What are the beneficial or detrimental effects of these interactions on complex sound representation in the auditory nerve? These questions are motivated by the need to explain the ability of the CNS to derive relatively stable percepts of complex sounds over wide ranges of intensity despite the apparent effects of the nonlinearity - a fact which suggests that we search for invariant aspects of the responses.

One such invarient parameter is the relative level of the primary components (Sec. III). Despite large variations in absolute levels of a two-tone stimulus, the ratio of the input levels (A_{in}/B_{in}) remains approximately preserved (or slightly enhanced in favor of the stronger tone) in the ratio of the output levels (A_{out}/B_{out}). This result becomes intuitive if we cast it in terms of the effect of the instantaneous nonlinearity on the shape of the compound waveform, u(t). From low to relatively high levels, and as g(u(t)) becomes progressively more saturated, the gross features of the compound waveform, especially the existence and positions of the peaks and troughs in the waveform, remain fairly intact. The relative level of the primary response components (A_{out}/B_{out}) simply reflects these stable features. In light of this, using the terms synchrony "suppression" or "capture" to describe these phenomena may be somewhat overstated, since the larger member of a two-tone complex does not dominate the output response of this nonlinear channel much more than it dominates the linear one. Instead, the "suppression" or "capture" behavior is largely a manifestation of the distortion in the absolute levels of the primary synchronous components.

These observations are illustrated in Fig.9, where the spatio-temporal responses of the model to two-tone (600 Hz, 1300 Hz) stimuli are plotted for 2 intensities. The relatively linear responses at the lowest intensity (Fig.9a) give way to the compressed response waveforms at the highest intensity. However, the patterns of response remain relatively stable; i.e., each tone dominates the synchronous responses in a certain broad region, with the transition regions (or borders) becoming somewhat more sharply defined. This is a direct reflection of the linear basilar membrane frequency selectivity which is preserved at all intensities only in the synchronous patterns across the hair cell and auditory-nerve-fiber array. At high intensities, the spatial profiles of the average (DC)

responses become essentially flat and saturated; the same applies to the absolute level of synchrony of each stimulus component in the region of its characteristic frequency location.

Therefore, at high intensities, it is impossible to utilize the above two measures (i.e. the spatial profiles of the average and of the absolute synchronous rates) to localize sufficiently the responses of each tone, and hence to use the tonotopic map (place code). Instead, various hypotheses have been advanced that make use of more robust temporal features of the responses with respect to the saturating nonlinearity, such as the frequency of the synchronous response. These algorithms either dispose of the tonotopic axis (e.g. the Dominant Frequency Algorithm; Sinex and Geisler, 1984; Delgutte, 1984), or impose an additional spatial selectivity (as in the ALSR; Young and Sachs, 1979). However, there are spatial features in the response patterns that are quite stable with intensity: for instance, the sharp borders or edges created by the transitions between different synchronous regions, and the rapid phase shifts occuring at or near the point of resonance of each stimulus component (Shamma, 1985a). The existence of these features depends on the integrity of the fine temporal responses of the auditory-nerve. Their extraction and localization along the spatial tonotopic axis can be accomplished by simple, purely spatial, edge detection algorithms, which can be implemented in the CNS as lateral inhibitory networks (Shamma, 1985b).

APPENDIX: Symbol List

Symbol	Meaning
a	parameter of the transducer nonlinearity. See Shamma et al. (1986) for biophysical interpretation.
A_{in}, B_{in} C_{in}	input amplitudes of tone-A, tone-B, and tone-C
A_{out}, B_{out} C_{out}	the amplitude of response components at the frequency of tone-A, tone-B, and tone-C
C_0, C_1	constants
C_a, C_b	effective capacitances of the hair cell
E_k	effective K^+ reversal potential
E_t	endocochlear potential
$g(u)$	dimensionless form of the nonlinearity
$\tilde{g}$	deviations of g(u) from rest
$G(u), G_0$ G_{max}	mechanical transducer conductance, its value at rest (G(0)), and its maximum value
G_1	parameter of the transduction nonlinearity. See Shamma et al. (1986) for biophysical interpretation.
G_k	K^+ ionic channel conductance
$\tilde{G}$	deviations of G from rest
j	$\sqrt{-1}$
$k(\omega)$	attenuation due to the hair cell membranes
n, N, M	positive integers
R	gas constant
t	time
t_1	time at which g(t) first exceeds u_o
t_2	time at which g(t) first falls below u_o

T	period
T_o	temperature
T_b	$2\pi/\omega_b$
u	cilia displacement
u_o	cilia displacement at maximum g(u) slope
u_a, u_b	cilia displacement due to tone-A and tone-B
v	dimensionless intracellular potential
$V, V_o, \tilde{V}$	intracellular potential, its rest value its deviations from rest
$V_{AC}, \tilde{V}_{AC}$	AC component of potential
$\tilde{V}_{DC}$	DC component of $\tilde{V}$ potential
W	basilar membrane displacement
α	phase shift
β	parameter of the transduction nonlinearity
θ	angle
τ	hair cell effective time constant
ω	frequency
$\omega_0, \omega_a, \omega_b$	fundamental frequency of a complex tone, frequency of tone-A and tone-B

REFERENCES

Delgutte B. (1984). "Speech coding in the auditory-nerve. II.Processing schemes for vowel-like sounds" J. Acoust. Soc. Am. 75(3), p. 879-886.

Engebretsen A. and Eldredge D. (1968). "Model for nonlinear characteristics of cochlear potentials," J. Acoust. Soc. Am. 44(2), p.548-554.

Geisler D. (1985). "Effects of a compressive nonlinearity in a cochlear model", J. Acoust. Soc. Am. 78(1), p.257-259.

Geisler C., Deng L., and Greenberg S. (1985). "Thresholds for primary auditory fibers using statistically defined criteria" J. Acoust. Soc. Am. 77, p. 1102-1109.

Hall J. (1977). "Two tone suppression in a nonlinear model of the basilar membrane," J. Acoust. Soc. Am. 61, pp. 802-810.

Horst J., Javel E., and Farley G. (1986) "Coding of spectral fine structure in the auditory-nerve. I. Fourier analysis of period and interspike interval histograms", J. Acoust. Soc. Am. 79(2), p. 398-416.

Horst J., Javel E. and Farely G. (1985). "New effects of cochlear nonlinearity in temporal patterns in auditory-nerve fiber responses to harmonic complexes", in Peripheral Auditory Mechanisms, edited by J. Allen, J. Hall, A. Hubbard, S. Neely, and A. Tubis. Springer-Verlag: New York (in press).

Javel E. (1981). "Suppression of auditory-nerve responses I: Temporal analysis, intensity effects and suppression contours", J. Acoust. Soc. Am. 69(6), pp.1735-1745.

Javel E., McGee J., Walsh E., Farley G., and Gorga M. (1983). "Suppression of auditory-nerve responses. II: Suppression threshold and growth, iso-suppression contours", J. Acoust. Soc. Am. 74(3), pp.801-813.

Javel E., McGee J., Walsh E. and Farely G. (1984). "Studies of synchrony suppression in normal and hearing-impaired cats". In Mechanisms of Hearing, edited by W. Webster and L. Aitkin. Monash University Press: Australia.

Kim, D. (1985). "Overview of nonlinear and active cochlear models". In Peripheral Auditory Mechanisms, edited by J. Allen, J. Hall, A. Hubbard, S. Neely, and A Tubis. Springer-Verlag: New York (in press).

Pfeiffer, R. (1970). "A model for two-tone inhibition of single cochlear-nerve fibers," J. Acoust. Soc. Am., 48(6), 1373-1378.

Sachs M. and Abbas P. (1976). "Phenomenological model for two-tone suppression," J. Acoust. Soc. Am. 60, pp.1157-1163.

Sachs M. and Kiang N. (1968). "Two-tone inhibition in the auditory-nerve", J. Acoust. Soc. Am. 45, pp.1120-1128.

Sachs M. and Young E. (1980). "Effects of nonlinearities on speech encoding in the auditory nerve", J. Acoust. Soc. Am. 68(3), p.858-874.

Sellick I. and Russell I. (1979). "Two-tone suppression in cochlear hair cells," Hear. Res. 1, p.227-236.

Shamma S. (1985a). "Speech processing in the auditory system. Part I: The representation of speech in the responses of the auditory-nerve", J. Acoust. Soc. Am. 78(5), pp.1612-1621.

Shamma S. (1985b). "Speech processing in the auditory system. Part II: Lateral inhibition and the central processing of speech evoked activity in the auditory-nerve", J. Acoust. Soc. Am. 78(5), pp.1622-1632.

Shamma S., Chadwick R., Wilbur J., Morrish K., Rinzel J. (1986). "A biophysical model of cochlear processing: Intensity dependence of pure tone responses", J. Acoust. Soc. Am. (in press).

Sinex D. and Geisler D. (1983). "Responses of auditory-nerve fibers to consonant-vowel syllables," J. Acoust. Soc. Am. 73(2), p.602-615.

Young E. and Sachs M. (1979). "Representation of steady state vowels in the temporal aspects of the discharge patterns of populations of auditory-nerve fibers," J. Acoust. Soc. Am. 60, pp.1381-1403.

Figure Legends:

Fig.1:

A schematic of the simplified biophysical model of the cochlear stages. All symbols are defined in the text.

Fig.2:

Two-tone synchrony suppression in the hair cell model.
(a) Synchrony/level functions of tone-A (600 Hz), with tone-B (700 Hz) cilia displacements (B_{in}) of 0.1, 0.2, 0.4, 0.8 and 1.6 μm from left to right.
(b) Corresponding suppression of tone-B synchronous responses (B_{out}) as a function of increasing A_{in}, with B_{in} of 0.1, 0.2, 0.4, 0.8, and 1.6 μm from bottom to top.

Fig.3(a,b):

Graphical representation of the transfer characteristics of the hair cell nonlinearity g(u) and its derivitive g'(u) with a sinusoidal input u_b.

Fig.4:

The change in the relative levels of the outpput synchronous components (A_{out}/B_{out}) as a function of the absolute level of the stimulus (~ B_{in}), with relative input levels (A_{in}/B_{in}) of 0.1, 0.25, 0.5, 0.66, 1, 1.33, 2, 3, 10 from bottom to top. The frequencies of the two tones are $\omega_a/2\pi$=600 Hz and $\omega_b/2\pi$=700 Hz.

Fig.5:

Two-tone synchrony suppression in the composite cochlear model.

(a) Iso-intensity tuning curves of tone-A synchronous responses in the absence of tone-B (B_{in}=0), with amplitude of tone-A stapes displacement of 0.05, 0.1, 0.2, and 0.4 μm from bottom to top.

(b) Same as above, but with cilia displacement B_{in} = 0.07 μm, and $\omega_b/2\pi$=1700 Hz

(c) Same as above, but with B_{in}=0.2 μm

(d) Same as above, but with B_{in}=0.4 μm

Fig.6:

Reciprocal suppression of tone-B (1600 Hz) synchronous outputs by tone-A stimuli shown in Fig.5.

(a) B_{out} suppression as a function of tone-A frequency, with tone-A stapes displacement of 0.05, 0.1, 0.2, and 0.4 μm from bottom to top, and B_{in}=0.07 μm

(b) same as above, but with B_{in}=0.2 μm.

(c) same as above, but with B_{in}=0.4 μm.

Fig.7:

Three-tone synchrony suppression. Each curve represents the synchronous responses due to tone-C (C_{out}) in the presence of an increasing tone-A cilia displacement level (A_{in}), with tone-B level (B_{in}) of 0.01, 0.1, 0.2, 0.4, and 0.8 μm from top to bottom. The frequencies are :$\omega a/2\pi$= 800 Hz, $\omega_b/2\pi$= 500 Hz, $\omega_c/2\pi$= 700 Hz.

Fig.8:

Output spectrum of a multi-component stimulus applied at the hair cell input with stimulus level as parameter. The stimulus has a flat spectrum composed of an 8-harmonic series of a 100 Hz fundamental (400-1100 Hz). Ain = .01, .02, .04, .08, .16, .32, .64, 1.28 μm from bottom to top.

Fig.9:

Spatio-temporal responses of the cochlear model to 600/1300 Hz stimulus at (a) low levels, and (b) high levels.

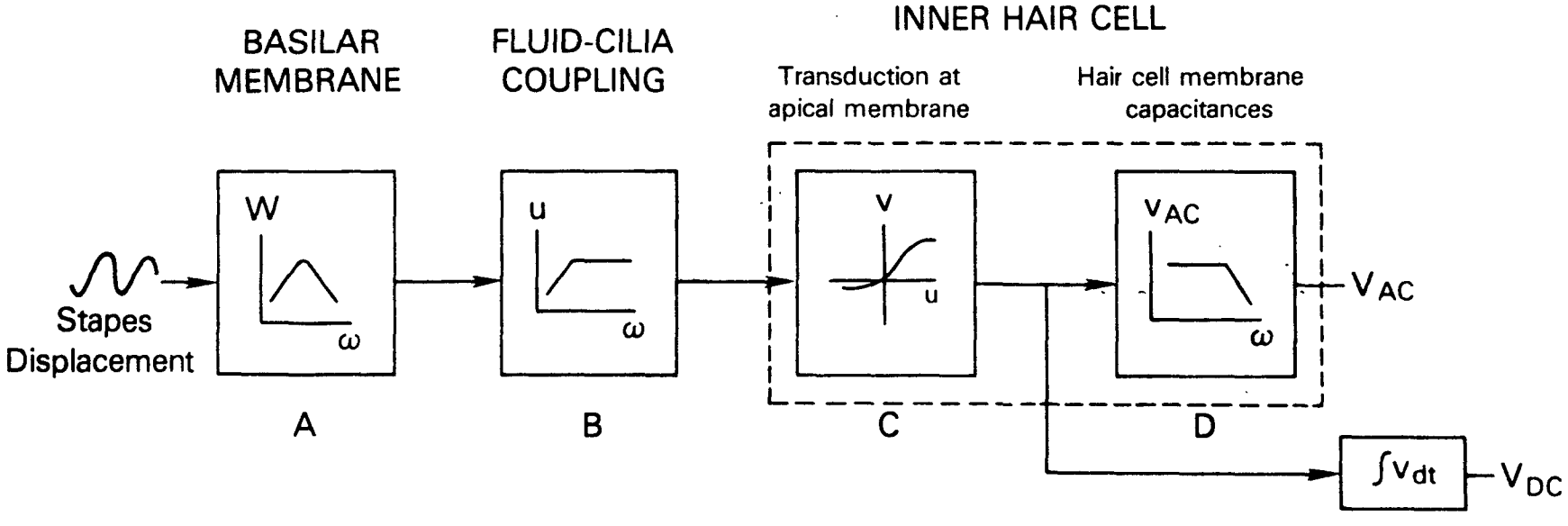
BASILAR MEMBRANE
FLUID-CILIA COUPLING
INNER HAIR CELL
Transduction at apical membrane
Hair cell membrane capacitances
W
ω
u
ω
v
u
V_{AC}
ω
V_{AC}
Stapes Displacement
A
B
C
D
$\int v\,dt$
V_{DC}

FIG. 1

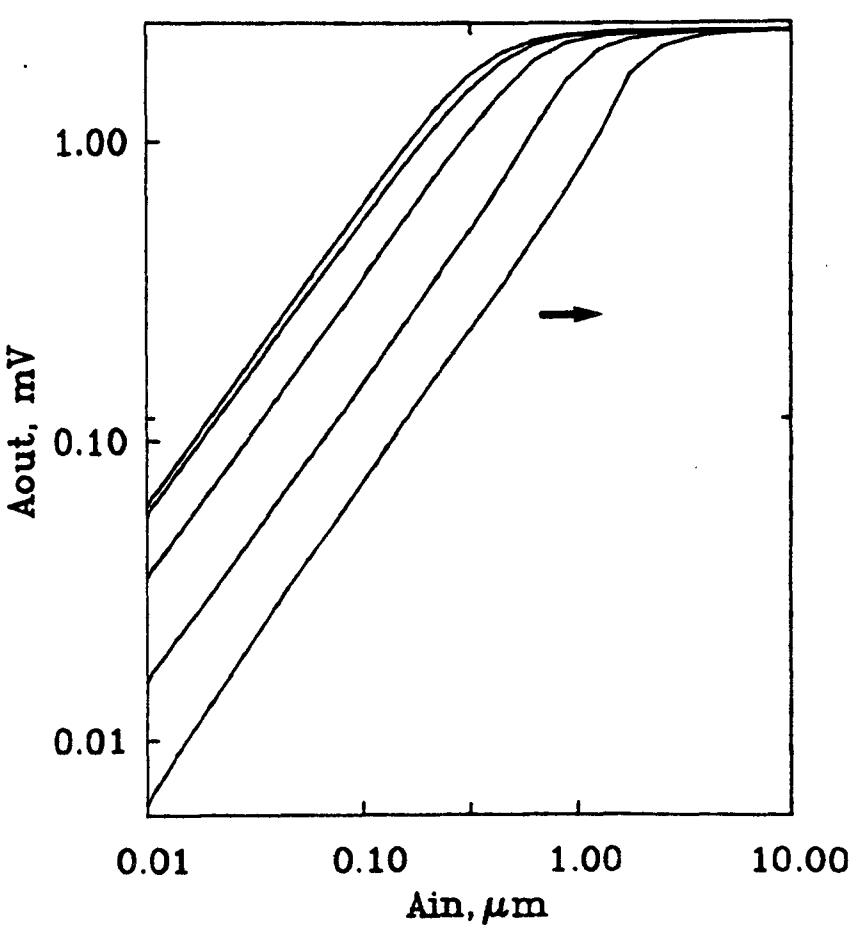
1.00
0.10
0.01
Aout, mV
0.01
0.10
1.00
10.00
Ain, μm

A

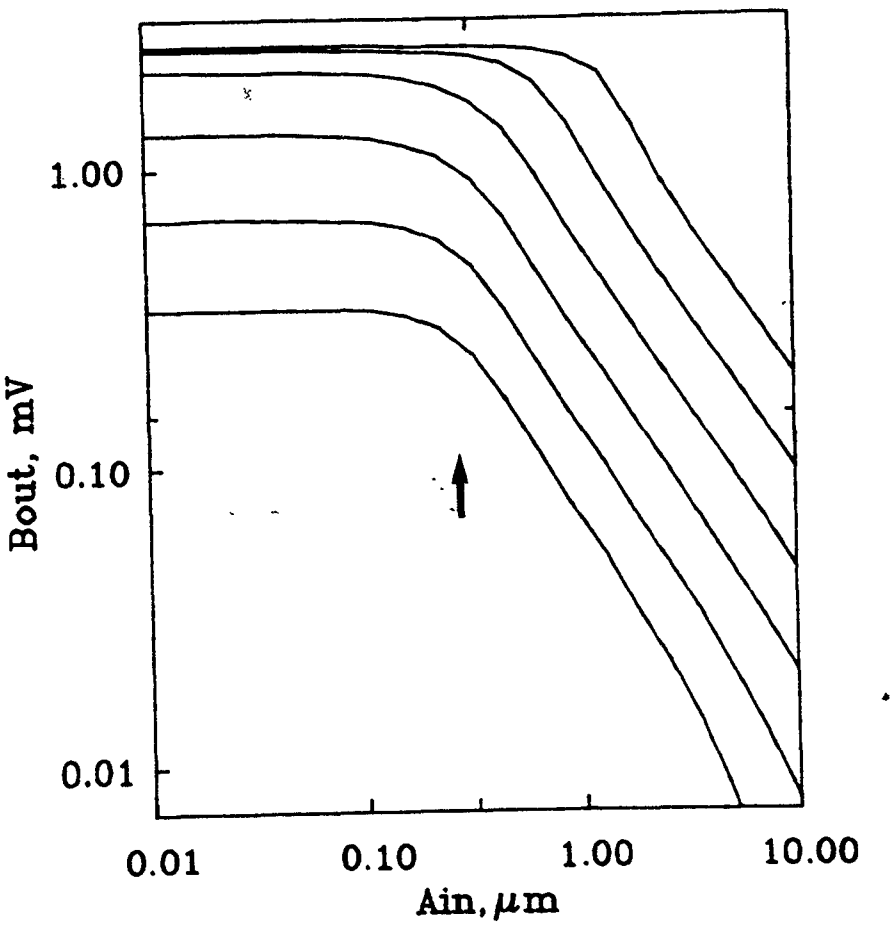
1.00
0.10
0.01
Bout, mV
0.01
0.10
1.00
10.00
Ain, μm

B

FIG. 2

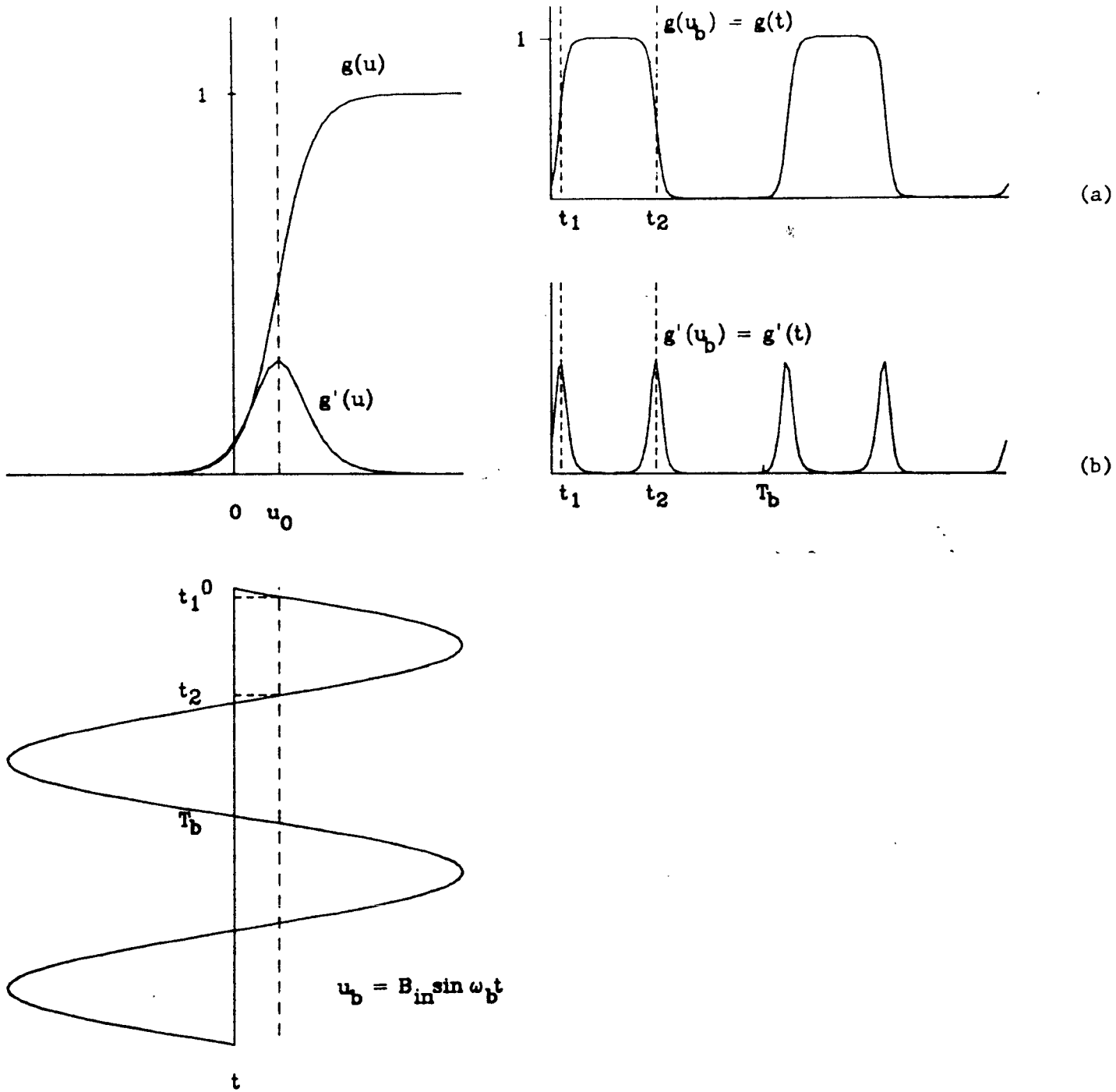
g(u)
1
g'(u)
0
u_0
$g(u_b) = g(t)$
1
t_1
t_2
(a)
$g'(u_b) = g'(t)$
t_1
t_2
T_b
(b)
t_1
0
t_2
T_b
$u_b = B_{in} \sin \omega_b t$
t

FIG. 3

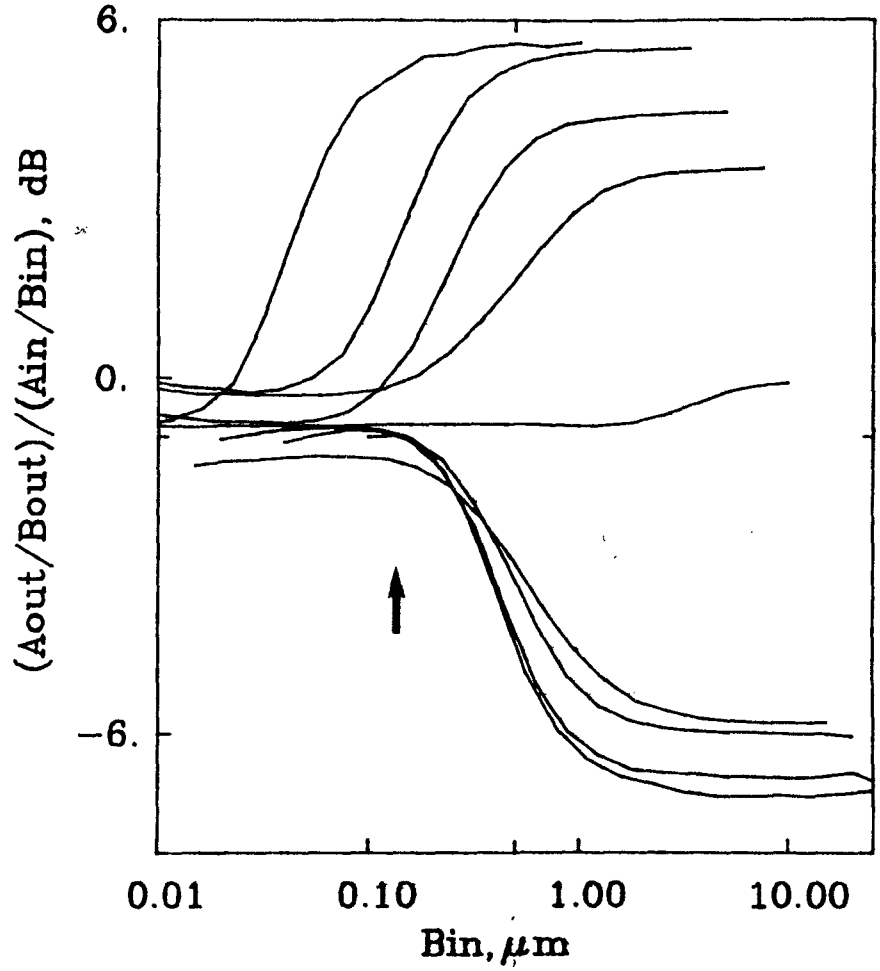

FIG. 4

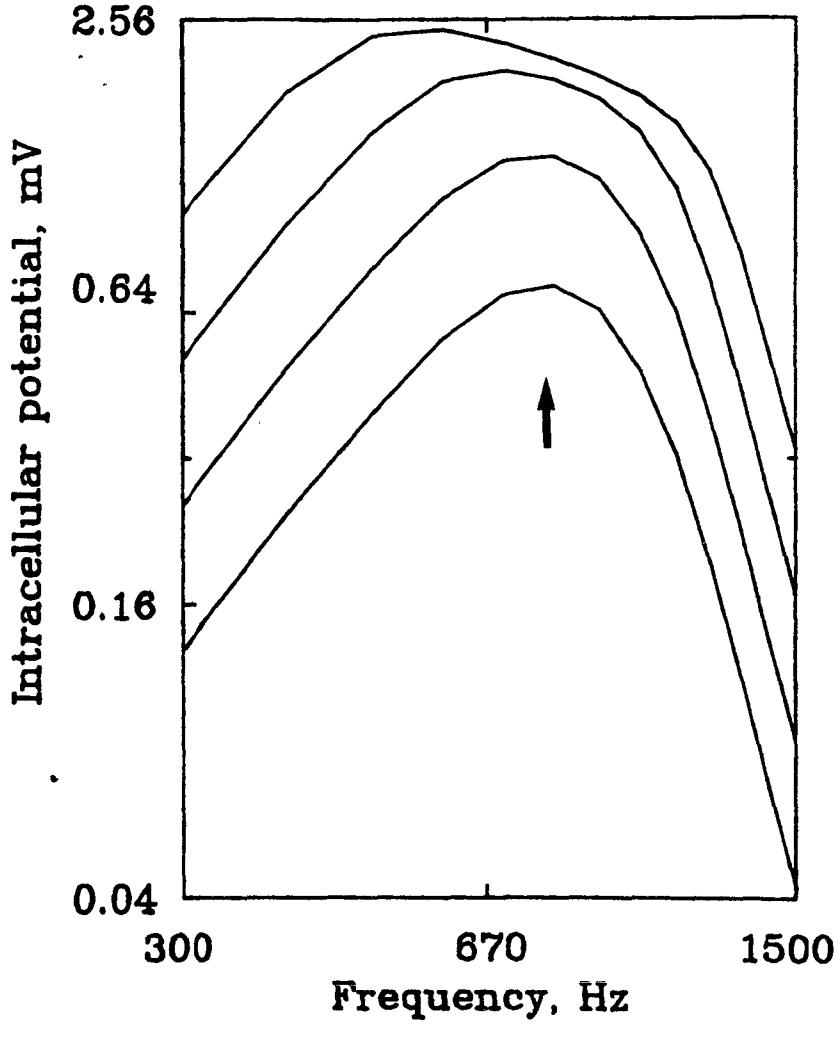
2.56
0.64
0.16
0.04
Intracellular potential, mV
300
670
1500
Frequency, Hz

A

FIG. 5

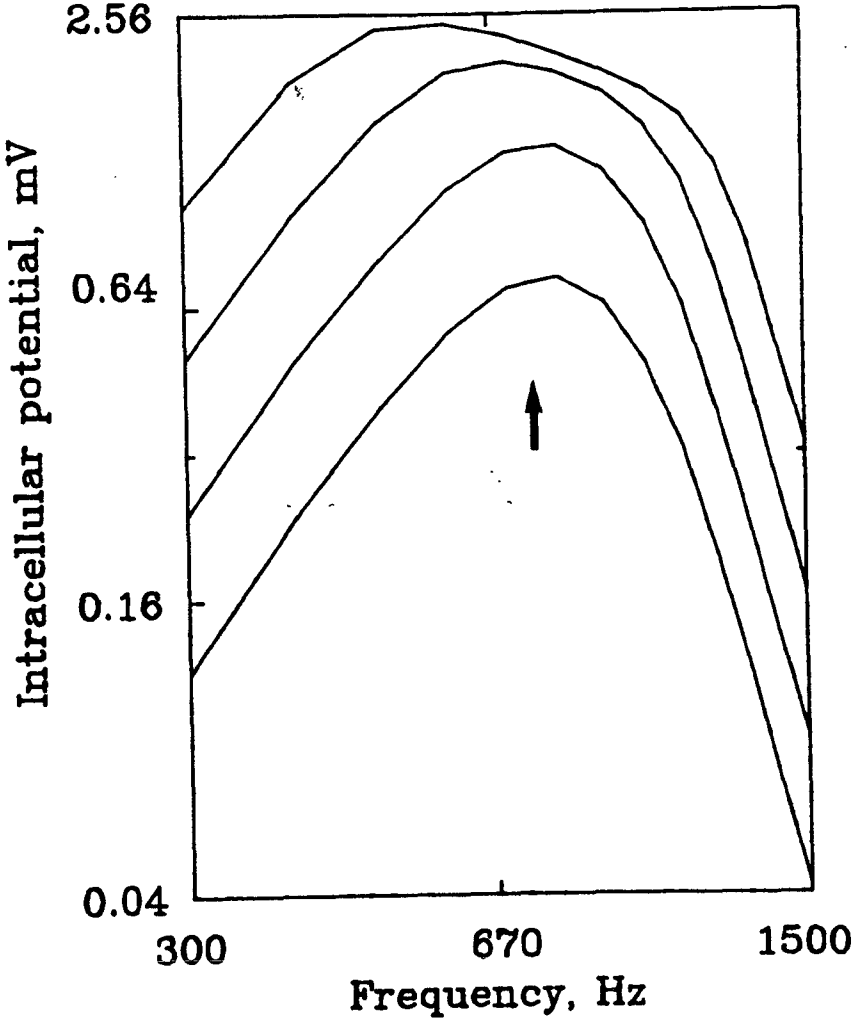
2.56
0.64
0.16
0.04
Intracellular potential, mV
300
670
1500
Frequency, Hz

B

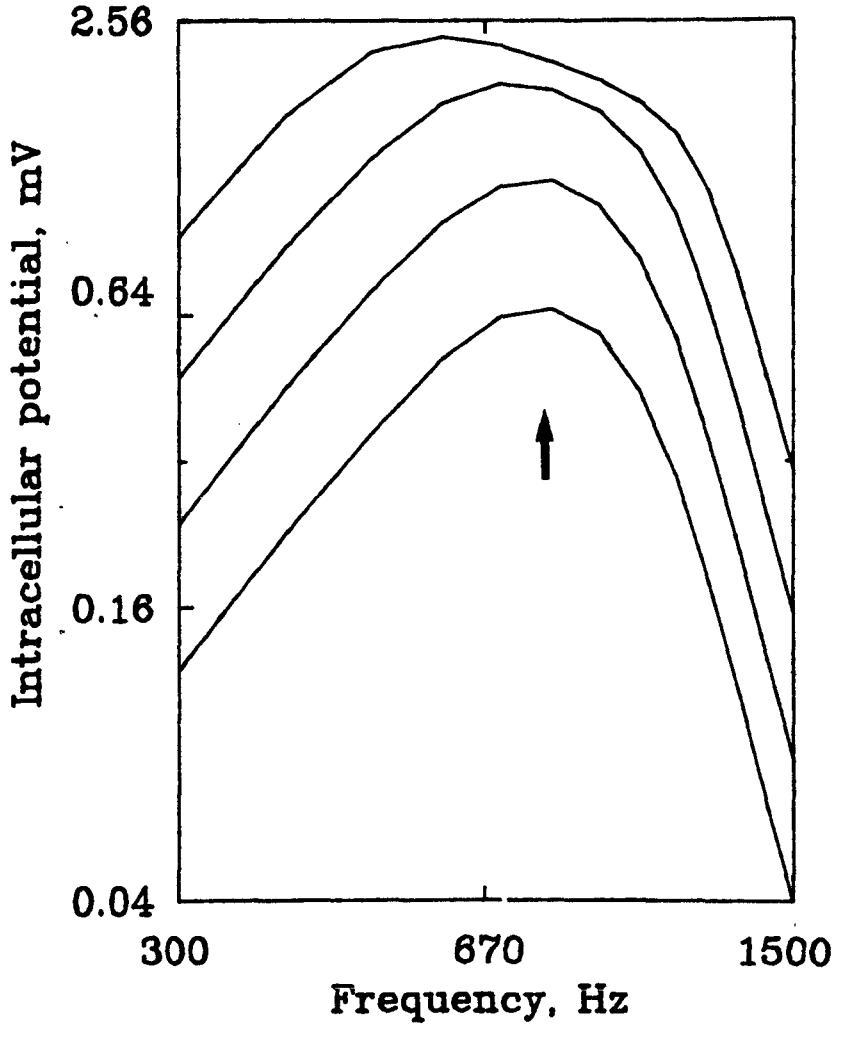
2.56
0.64
0.16
0.04
Intracellular potential, mV
300
670
1500
Frequency, Hz

C

FIG. 5

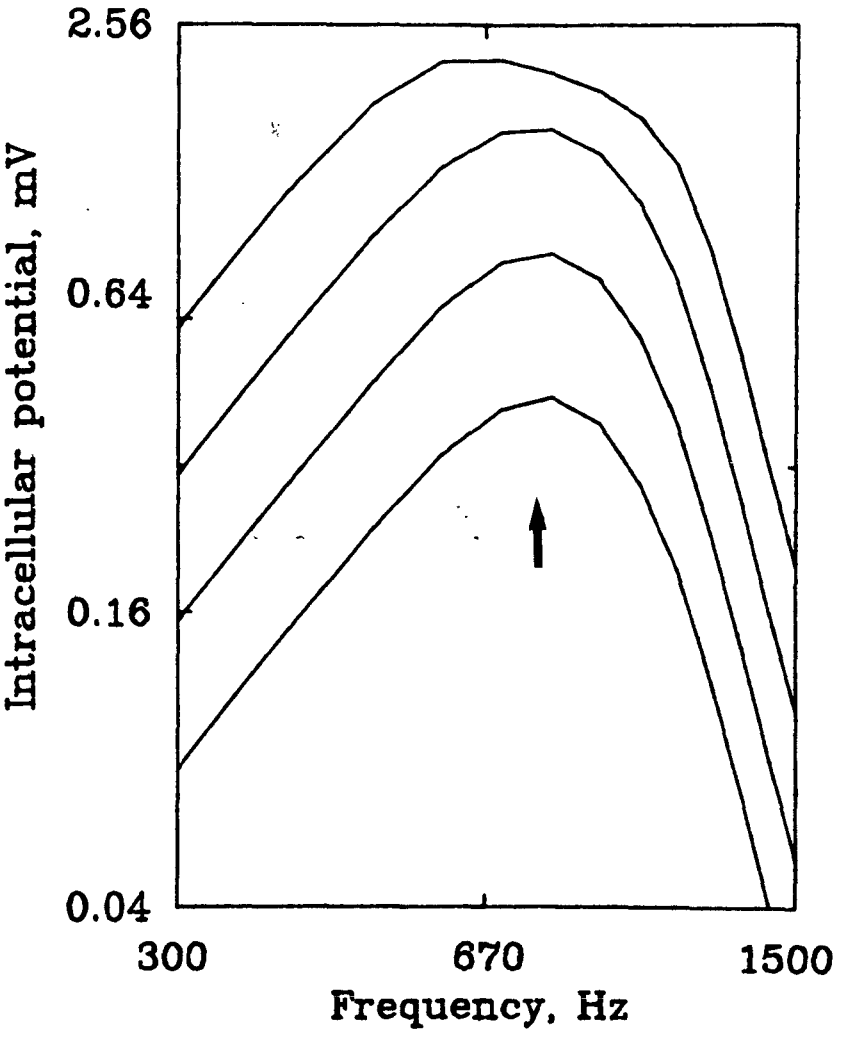
2.56
0.64
0.16
0.04
Intracellular potential, mV
300
670
1500
Frequency, Hz

D

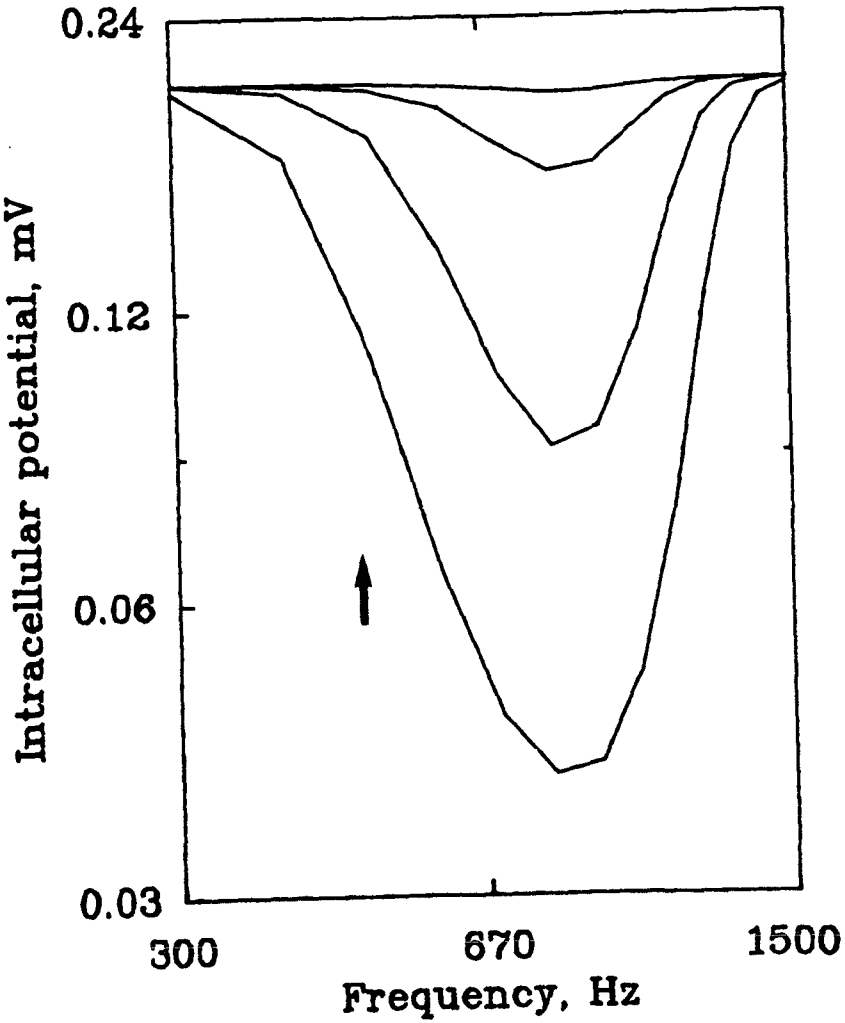
0.24
0.12
0.06
0.03
Intracellular potential, mV
300
670
1500
Frequency, Hz

A

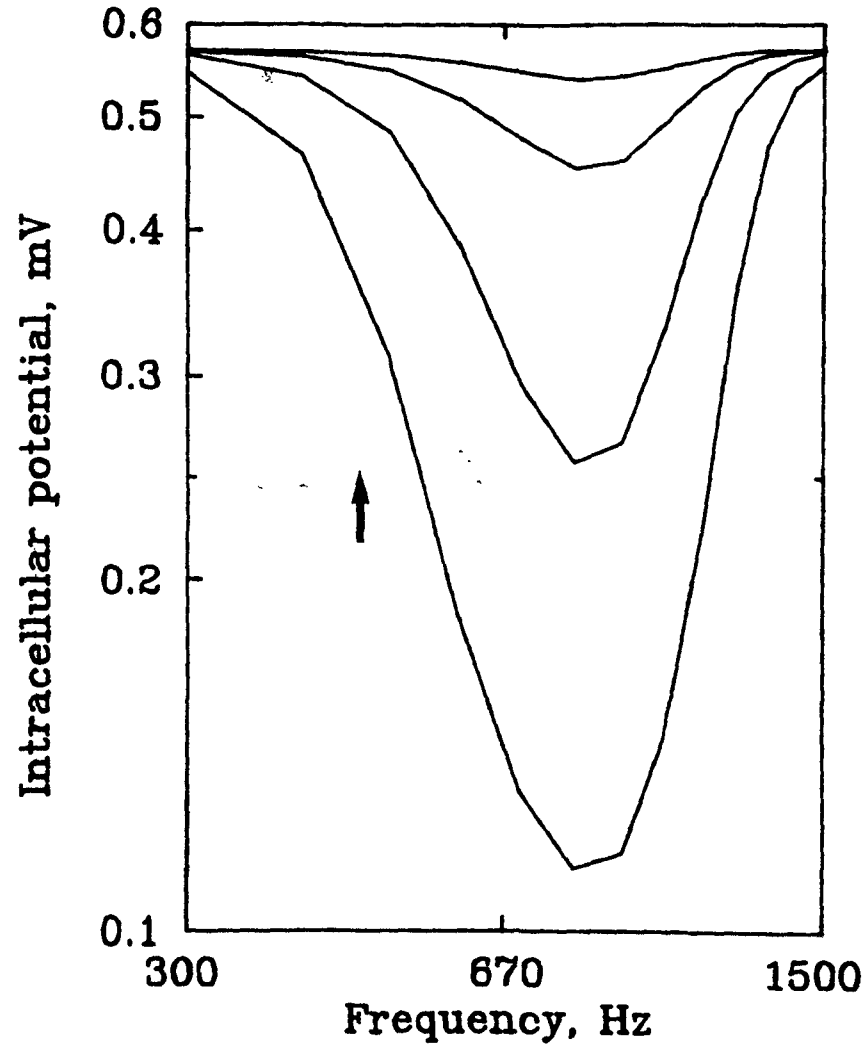
0.6
0.5
0.4
0.3
0.2
0.1
Intracellular potential, mV
300
670
1500
Frequency, Hz

B

FIGURE 6

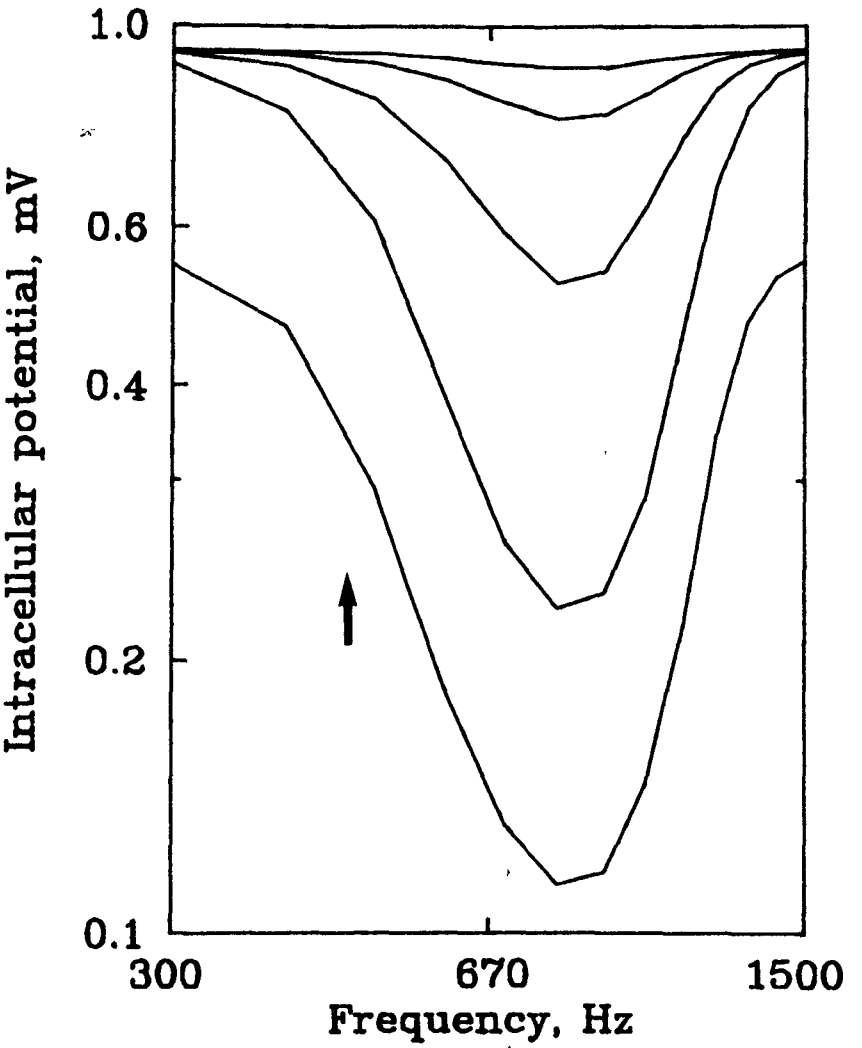
1.0
0.6
0.4
0.2
0.1
Intracellular potential, mV
300
670
1500
Frequency, Hz

FIGURE 6 C

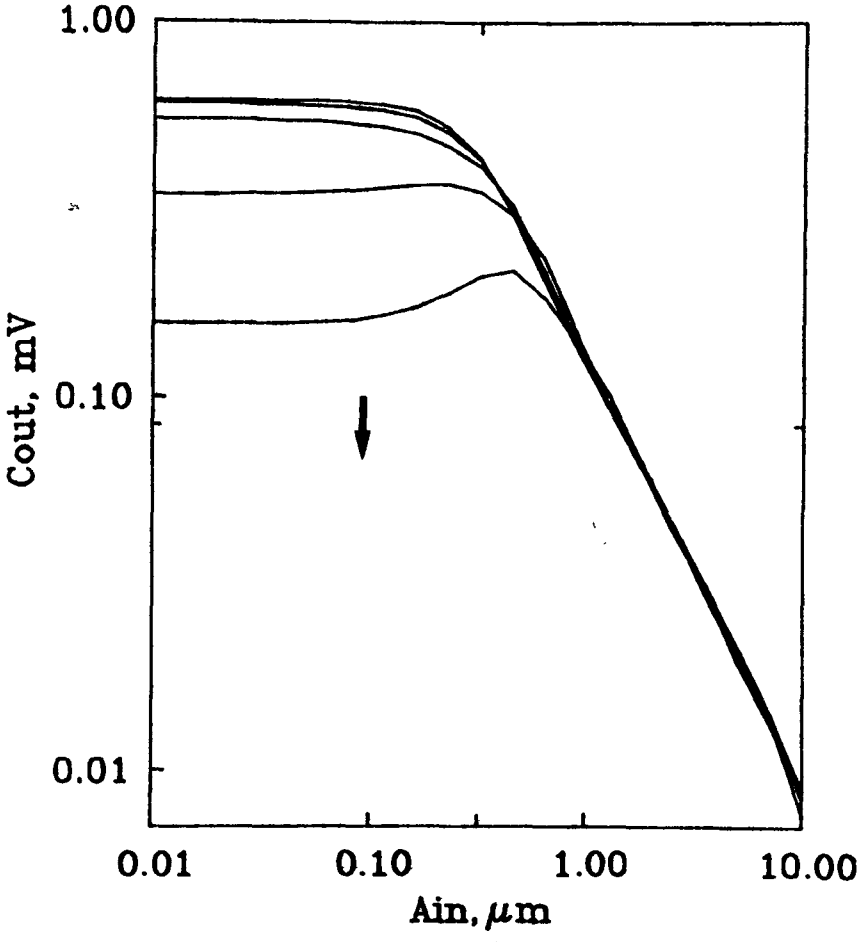

FIGURE 7

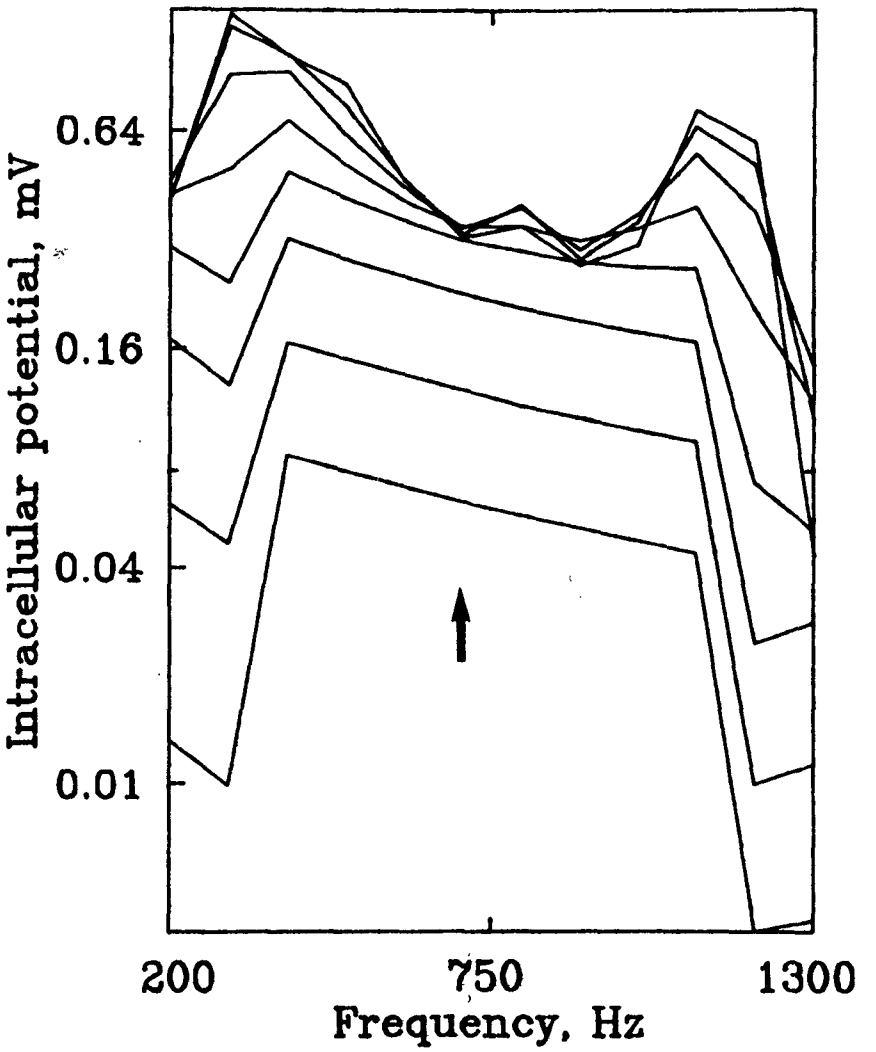
0.64
0.16
0.04
0.01
Intracellular potential, mV
200
750
1300
Frequency, Hz

FIGURE 8

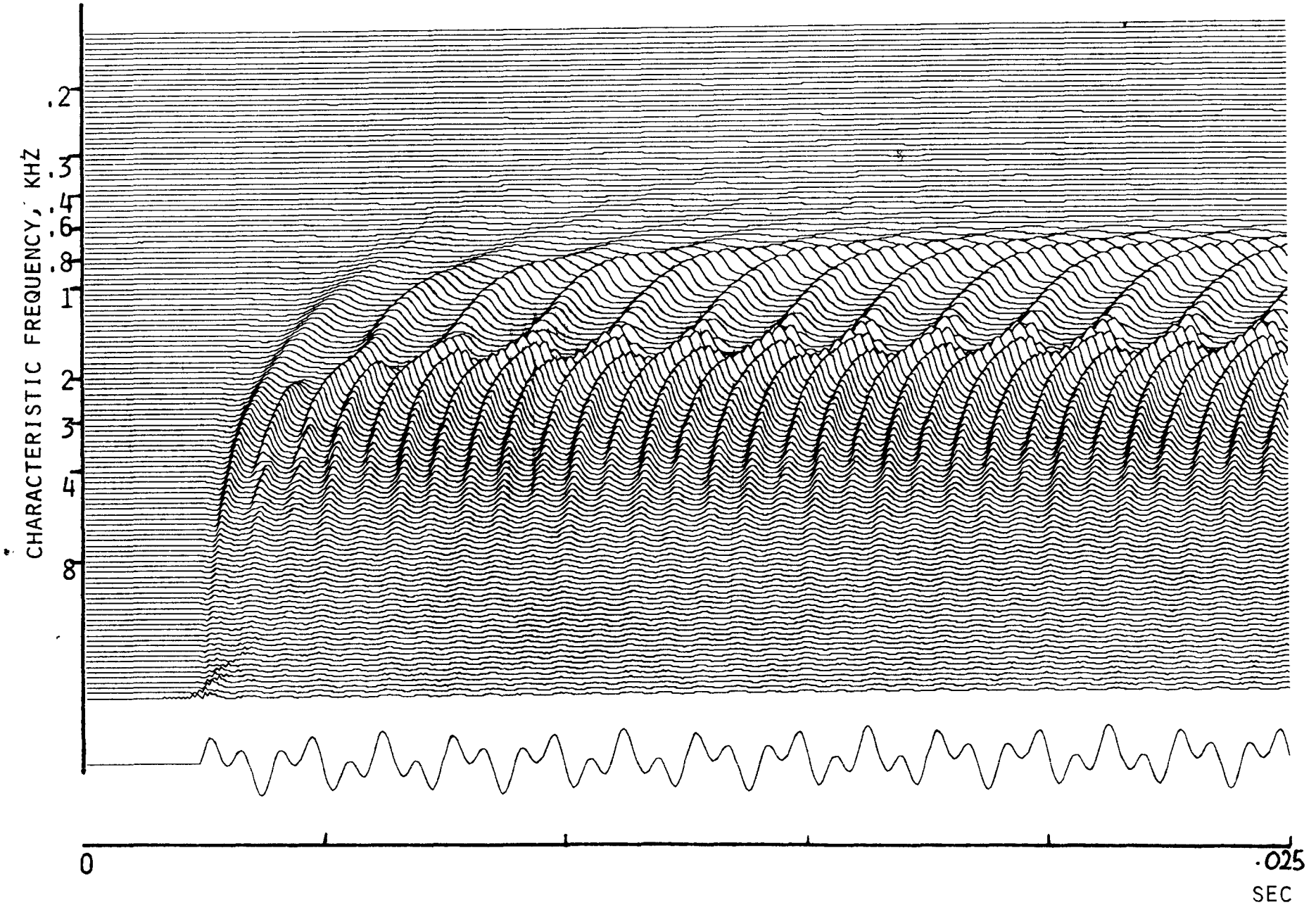

FIGURE 9 A

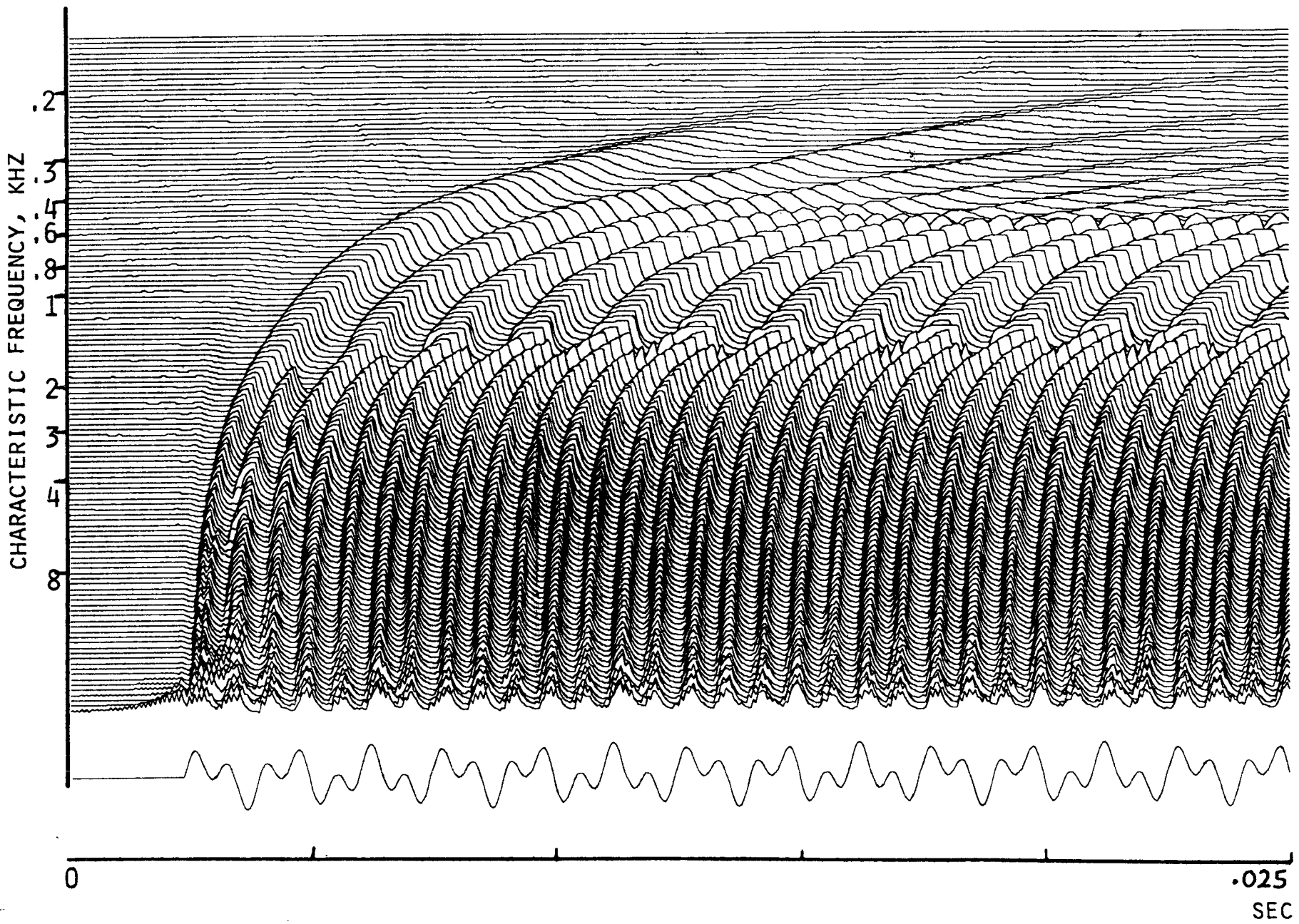

FIGURE 9 B